JOURNAL OF MATERIALS SCIENCE 23 (1988) 272–280

Indentation fracture in the $In_{1-x}Ga_xAs_yP_{1-y}$/InP system and its effect on microhardness anisotropy characteristics

D. Y. WATTS*, A. F. W. WILLOUGHBY
Engineering Materials, the University, Southampton, S09 5NH, UK

Knoop microhardness anisotropy measurements on the {1 0 0}-orientated $In_{1-x}Ga_xAs_yP_{1-y}$/InP system have disclosed an appreciable variation in hardness behaviour across the composition range of the alloy. This paper relates these variations to changes in the directional fracture characteristics of the system. The qualitative investigation of both Vickers and Knoop indentation fracture has established the emergence of a secondary ⟨1 0 0⟩ cleavage direction at high values of the composition parameter, above $y \simeq 0.6$. Furthermore, the number and extent of cracks emanating from indentations were seen to increase appreciably as y increases from 0 to 1. A quantitative analysis of Vickers indentation fracture in the quaternary system has indicated a marked dependence of fracture-related parameters on both the indentor orientation and composition. Fracture toughness values from $\sim 3.10^5$ to $\sim 1.10^6$ N m$^{1/2}$ have been derived using expressions from the literature. The marked change in Knoop microhardness anisotropy characteristics with increasing y in the $In_{1-x}Ga_xAs_yP_{1-y}$/InP system has been partially correlated to the emergence of ⟨1 0 0⟩ cleavage and the general increase in indentation fracture, highlighted by the quantitative fracture measurements. Thus, it is concluded that even at very low indentation loads, the effect of fracture on the measured hardness of crystalline materials cannot be ignored.

1. Introduction

The Knoop microhardness anisotropy characteristics of the {1 0 0}-oriented $In_{1-x}Ga_xAs_yP_{1-y}$/InP quaternary system have already been measured and reported [1–3], and compared with earlier work. The results are not extensively described here, but are summarized in Fig. 1, which shows in three dimensions the Knoop hardness number (KHN) as a function of azimuthal indentor orientation (θ) and composition (y; the composition parameter referred to in the quaternary formula $In_{1-x}Ga_xAs_yP_{1-y}$, and related to x by the relation $y \simeq 2.1x$ as a prerequisite for lattice matching to an InP substrate). Fig. 2 shows the hardness data more clearly in two dimensions, with the KHN plotted against θ for the various compositions. θ refers to the angle between the Knoop indentors' long diagonal and an arbitrary ⟨1 1 0⟩ direction lying in the {1 0 0} surface of the sample.

The hardness anisotropy characteristics at $y = 0$ (InP) were seen to be similar to those earlier reported by Brasen [4, 5] although significant differences emerged. However, the overall trends in the two sets of data were consistent with a maximum in hardness at $\theta = 45°$ (i.e. the indentors' long diagonal aligned along a ⟨1 0 0⟩ direction) and hardness minima towards adjacent ⟨1 1 0⟩ directions. Extensive analyses [6] have compared the data with theoretical Knoop hardness anisotropy (KHA) curves predicted by some of the more well-established KHA models [7–11], and while some discrepancies emerged, a general agreement was obtained in most cases.

As y increases in the $In_{1-x}Ga_xAs_yP_{1-y}$/InP system the hardness anisotropy behaviour is seen to alter appreciably (see Figs 1 and 2). The most striking change is the emergence of a minimum in hardness in the $\theta = 45°$ (⟨1 0 0⟩) orientation where previously a maximum had been observed, creating two new hardness maxima at either side, approximately 23° from adjacent ⟨1 1 0⟩ directions. This new behaviour was predicted by none of the KHA theories, having assumed that the {1 1 1} $a/2$ ⟨1 1 0⟩ slip system predominates across the complete composition range (as observed by TEM studies [12, 13]).

The possibility that the change in hardness anisotropy characteristics might be attributable to a change in slip behaviour across the quaternary system has been investigated with a series of preferential etching experiments [6], with no ⟨1 0 0⟩ slip lines being observed in the {1 0 0} plane which would be necessary to predict this behaviour using the KHA theories (see [3]). Indentations made at an angle of $\theta = 45°$ at 260° C in InP and $In_{0.66}Ga_{0.34}As_{0.71}P_{0.29}$ are compared in Fig. 3. (The elevated indentation temperature greatly increased the amount of slip observed, but was assumed to be insufficiently high to affect the nature of the operative slip system.) The indentations in InP

Present address: STC Optical Devices Division, Brixham Road, Paignton, Devon TQ4 7BE, UK.

0022–2461/88 $03.00 + .12

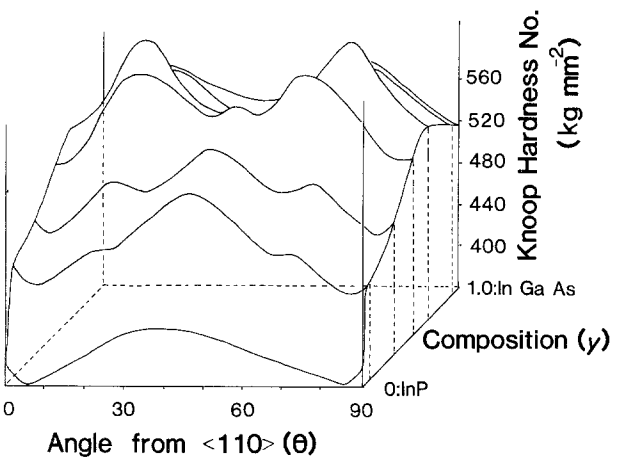

Figure 1 Knoop hardness as a function of indentor orientation and composition in the $In_{1-x}Ga_xAs_yP_{1-y}$/InP system.

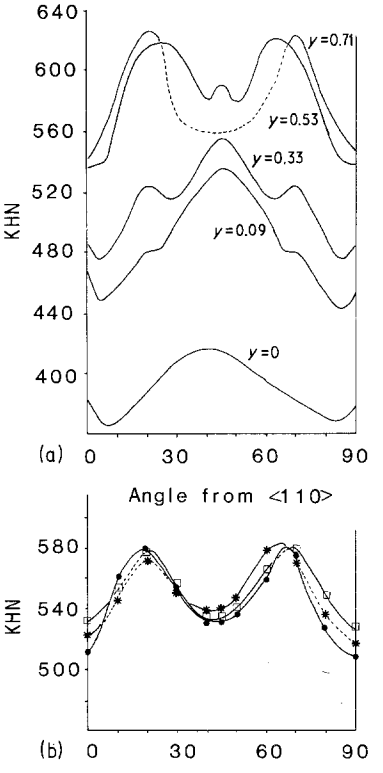

Figure 2 The Knoop hardness anisotropy of the $In_{1-x}Ga_xAs_yP_{1-y}$/InP system. y = (●) 0.745, (□) 0.92, (∗) 1.0.

have been etched in a 2 : 2 : 1 solution of $HBr : H_3PO_4 : H_2O$ for 25 sec at room temperature. The indentations in InGaAsP have been etched in a solution of 100 ml H_2O : 8 g KOH : 0.5 g $K_3Fe(CN)_6$ at room temperature for 10 min under 15 W tungsten filament lamp illumination (as reported by Lourenco [14]). The delineated etch pit patterns in the two materials are very similar, each clearly showing the two orthogonal $\langle 1\,1\,0 \rangle$ slip directions and leading to the conclusion that a change in slip behaviour is unlikely to be the reason for the variation in hardness anisotropy characteristics in the $In_{1-x}Ga_xAs_yP_{1-y}$/InP system. Accordingly, attention turned towards other possible explanations for the hardness behaviour. Firstly, elasticity was considered. Indentations, particularly those made at very low loads, have been seen to be susceptible to elastic recovery when the indentor is removed from the sample [15]. This produces a slightly smaller indentation than normal, with a correspondingly higher hardness value. At higher loads, the effect of elastic recovery becomes proportionately less and so a lower hardness value is obtained. However, while the Vickers hardness test has been seen to be affected by elastic effects at low loads, the Knoop indentor, due to its anisotropic shape, appears to be largely independent of such effects, experiencing little elastic recovery even at low loads. Finally, having noticed the appreciable amount of cracking associated with hardness indentations, even at low loads, it was felt that a detailed analysis of the indentation fracture characteristics in these materials might go some way towards accounting for the hardness behaviour.

2. Indentation fracture

While the field of hardness anisotropy has been investigated extensively, the related field of indentation fracture has been comparatively overlooked in the past. As Lawn and Wilshaw say, in their review of indentation fracture [16] "the characteristic microcrack patterns associated with indentations tend to be viewed at best as something of a curiosity, more often as a disruptive element to be avoided at all costs". Certainly, previous hardness anisotropy measurements (e.g. [7, 17]) have tended to ignore the possible effects of fracture, dismissing them, along with twinning and work-hardening, as too small to significantly affect the hardness readings. Bearing in mind the relatively high brittleness of some of ionic and covalent crystals studied, this seems an important omission. The investigation of indentation fracture, however, began over a hundred years ago with Hertz's analysis

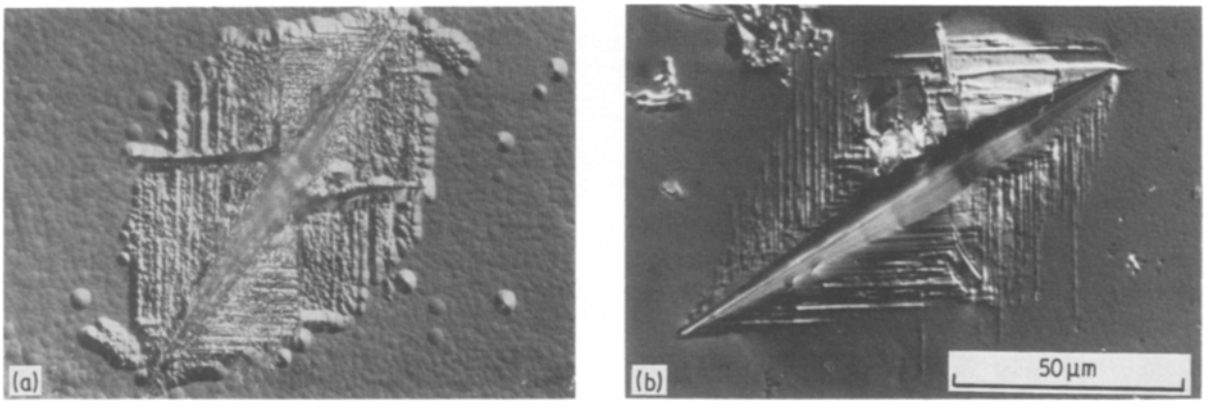

Figure 3 Etched high-temperature Knoop indentations in (a) InP and (b) $In_{0.66}Ga_{0.34}As_{0.71}P_{0.29}$.

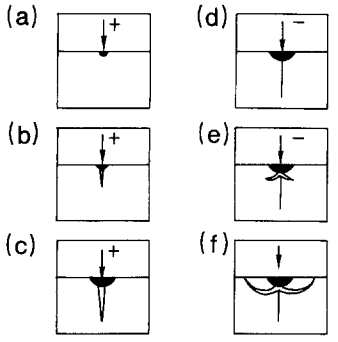

Figure 4 The geometry of cracks formed during "sharp" indentation, after Lawn and Swain [23].

of the elastic contact between two curved bodies [18]. By considering the nature of the stress field created by the two bodies under load, Hertz qualitatively predicted the nature of cracking seen to appear in one of the bodies. Similar work by Boussinesq [19] addressed the problem of fracture caused by "sharp" (pointed) indentors, but despite numerous reported observations of cracks emanating both outwards and below indentations (e.g. [20–22]), the field of indentation fracture remained relatively undeveloped until the 1970s. Lawn and Wilshaw then published a review of the principles and applications of indentation fracture [16] in which they derived expressions describing the nucleation, propagation and geometry of indentation-induced cracks. These are used to analyse fracture data, reported here, in Section 4.

The geometry of cracks formed during "sharp" indentation was schematically described by Lawn and Swain [23] and is illustrated in Fig. 4. In the diagram, the caption letters (a) to (f) refer to the following stages:

(a) Initial loading: the sharp indentor produces a region of plastic deformation in the vicinity of the contact point.

(b) Critical zone formation: at some threshold indentation load a crack suddenly initiates below the contact point, where the stress concentration is greatest. This crack is called the median vent.

(c) Stable crack growth: the increasing load causes further stable extension of the median vent.

(d) Initial unloading: on unloading, the median vent begins to close (but not heal).

(e) Residual-stress cracking: the relaxation of the deformed material within the contact zone just prior to the removal of the indentor superimposes intense residual tensile stresses upon the applied field. Sideways-extending cracks, called lateral vents, begin to appear.

(f) Complete unloading: upon complete removal of the indentor, the lateral vents continue their expansion, towards the specimen surface.

Experimental observations of indentation fracture have corroborated this account of crack formation and geometry. Lawn and Fuller [24] commented on the "half penny" configuration of lateral cracks which reach the surface of the sample, while Hockey and Lawn [25] provided TEM evidence supporting the Lawn and Swain cracking configuration. Further fracture observations (e.g. [26, 27]) indicate the cracking model to be a reliable one. More recently, median and lateral vents produced in germanium under a range of conditions were examined by Roberts *et al.* [28], who established that the ductile/brittle transition temperature in doped germanium was markedly different for n- and p-type dopants. Several workers have sought to quantify the fracture produced during indentation, and this work is discussed with respect to these authors' results in Section 4.

3. Experimental details

The experimental work divided broadly into two groups: firstly a qualitative analysis of the indentation fracture geometry in the $In_{1-x}Ga_xAs_yP_{1-y}$/InP system, and secondly a quantitative approach, seeking to derive some of the fracture-related parameters of the material. The cracking data tend to be somewhat extensive and so written description is kept to a minimum.

The samples used are listed in Table I, comprising a bulk sample of InP (B–IP–1) and liquid-phase expitaxy (LPE)-grown layers of $In_{1-x}Ga_xAs_yP_{1-y}$/InP with composition parameters of $y = 0.27$ (sample Q–IGAP–2); $y = 0.62$ (Q–IGAP–3); $y = 0.9$ (Q–IGAP–4) and $y = 1.0$ (T–TGA–5: the lattice-matched ternary alloy $In_{0.53}Ga_{0.47}As$). All the available information on these samples is summarized in Table I.

Both Vickers and Knoop indentation fracture have been investigated using a Matsuzawa MHT-1 microhardness equipped with the appropriate diamond

TABLE I All samples have been supplied by STL (Harlow) or by the SERC III-V facility at Sheffield (US) and are within 2° of ⟨100⟩ surface orientation. All samples were fully polished on delivery and required no further preparation prior to use. Composition parameters (x and y) were determined by the suppliers using infrared transmission characteristics. All layers were grown by LPE

Sample number	Supplier	Layer (L) or bulk (B)	Composition		Quoted carrier concentration (cm^{-3}) at room temp.	Quoted etch pit density	Layer thickness (μm)
			x	y			
B–IP–1	STL	B	0	0	1.5×10^{16}	10^3	–
Q–IGAP–2	US	L	0.13	0.27	–	"zero"	4.5
Q–IGAP–3	STL	L	0.30	0.62	1×10^{17}	–	2.5
Q–IGAP–4	STL	L	0.43	0.90	5×10^{17}	–	3.5
T–IGA–5	STL	L	0.475	1	7.5×10^{15}	"high"	1.75
Q–IGAP–6	STL	L	0.32	0.71	1.1×10^{16}	10^3	5.5
Q–IGAP–7	US	L	0.047	0.1	–	–	5
Q–IGAP–8	STL	L	0.15	0.34	10^{16}–10^{17}	–	7.5
Q–IGAP–9	STL	L	0.24	0.53	10^{16}–10^{17}	–	8.5
Q–IGAP–10	US	L	0.44	0.92	10^{16}–10^{17}	–	6.1

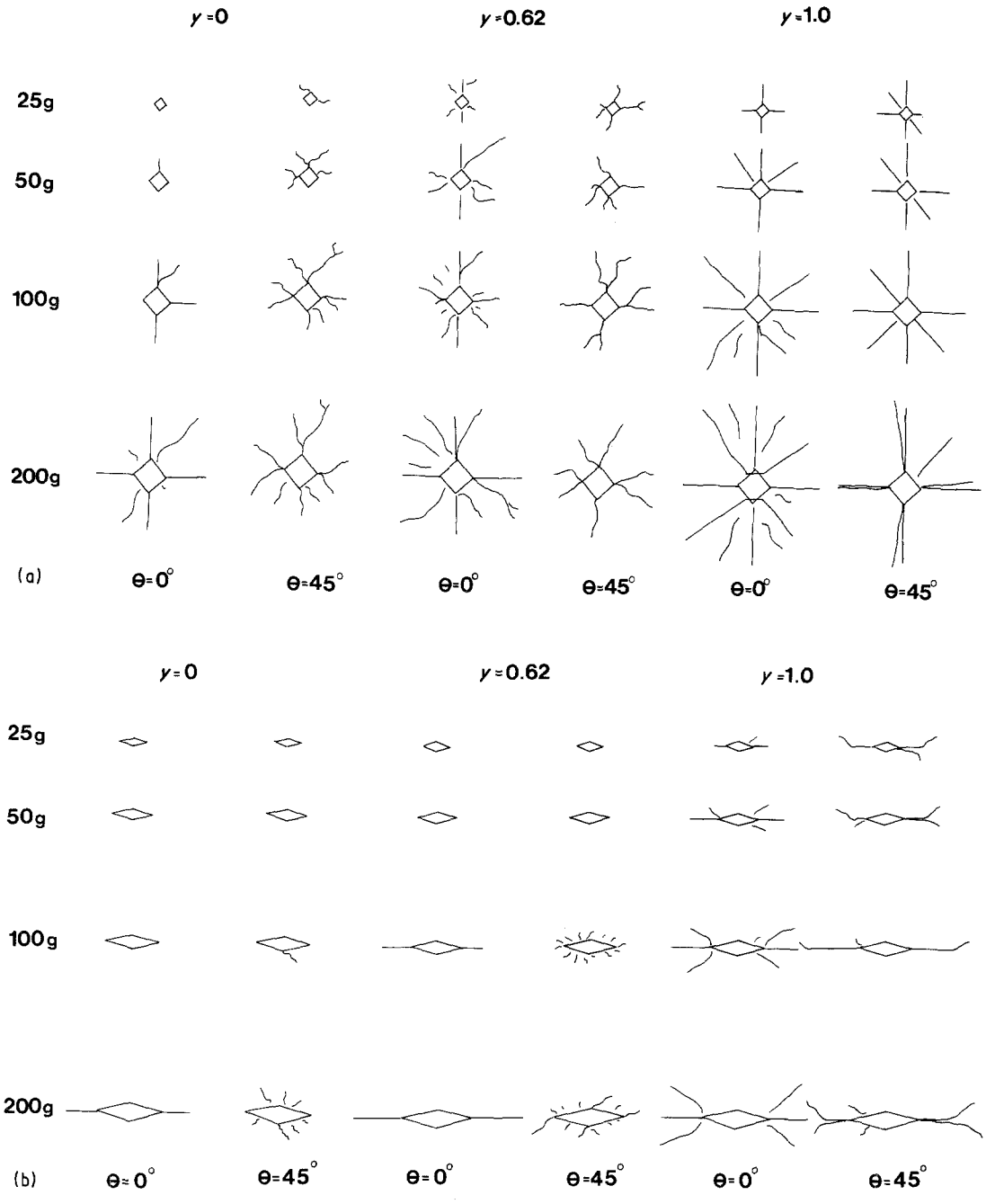

Figure 5 (a) Vickers and (b) Knoop indentation fracture in the $In_{1-x}Ga_xAs_yP_{1-y}$/InP system.

indentor. All indentations were made at room temperature in air, with an indentor "dwell-time" of 15 sec.

3.1. Qualitative indentation fracture analysis

3.1.1. Surface indentation fracture analysis

The geometry of indentation-induced cracks in the surface of the previously listed samples was examined at loads of 25, 50, 100, 200 and 300 g, together with indentor orientations of $\theta = 0°$ and 45° (Vickers) and $\theta = 0°$, 22.5° and 45° (Knoop). The cracking is comprehensively illustrated in [6], while Fig. 5 schematically represents the most relevant fracture geometries, corresponding with the important observations of the cracking behaviour, which are listed below.

1. The indentation of InP (both Vickers and Knoop) produced microcleavage cracks in $\langle 1\,1\,0 \rangle$ directions, while in $In_{1-x}Ga_xAs_yP_{1-y}$/InP layers of $y > 0.6$ there were signs of cleavage cracks in $\langle 1\,1\,0 \rangle$ directions, and additionally, $\langle 1\,0\,0 \rangle$ directions, particularly in the $\theta = 45°$ orientation.

2. The indentation-induced fracture was seen to increase in extent as y increased from 0 to 1.

3. The fracture associated with $\theta = 45°$ indentations (both Vickers and Knoop) was seen to occur at generally lower loads than that in the $\theta = 0°$ indentor orientation, at all compositions.

Two further observations made during this investigation [6] are worth mentioning at this point:

1. Room-temperature Vickers indentations in InP showed a marked "pin-cushion" and "barrel" shape for $\theta = 0°$ and 45° indentation orientation, respectively. This effect, described by Tabor [15] results in the nominally straight indentation edges being concave and convex for $\theta = 0°$ and 45° indentations. This effect was not observed during the Vickers indentation of $In_{1-x}Ga_xP_{1-y}$/InP layers.

2. Room-temperature indentation produced small

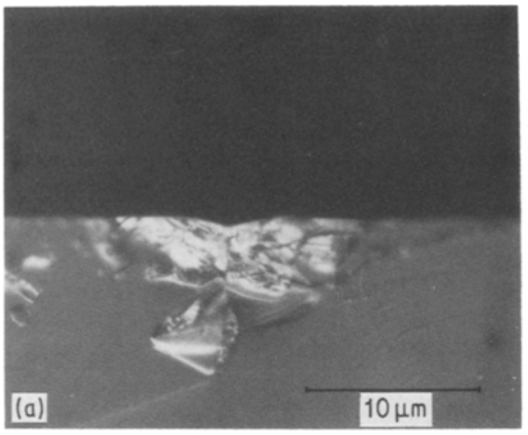

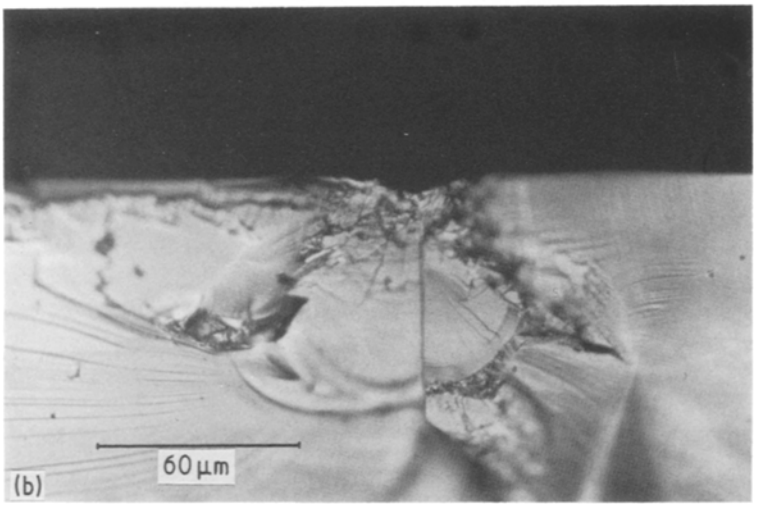

Figure 6 Cross-sectional micrographs of Vickers indentations made in InP at room temperature and at loads of (a) 25 g and (b) 200 g.

(but significant) amounts of slip in InP (as revealed by preferential etching) while in $In_{0.53}Ga_{0.47}As$, observable amounts of slip were not produced.

3.1.3. Cross-sectional indentation fracture analysis

In order to examine the cross-sectional indentation fracture geometry in the $In_{1-x}Ga_xAs_yP_{1-y}$/InP system, it was necessary to cleave directly through the centre of indentations, typically of the order of only a few tens of micrometres across. This was achieved by using the Knoop indentor as a "cleavage tool"; three or four Knoop indentations were made at high load (300 g) which all lay along a $\langle 1\,1\,0 \rangle$ cleavage direction and were all joined at the ends. Further along the same cleavage line lay the indentation to be sectioned, having been able to align the Knoop indentations exactly because of the accuracy of the MHT-1 microhardness tester. Applying a small bending moment produced the desired cleavage.

Fig. 6 shows section micrographs of Vickers indentations made in InP at room temperature and at loads of 25 and 200 g. The region of plastic deformation and the median vent (as described by Lawn and Swain [23]) can clearly be seen in both cases, with the lateral vents only apparent in the high load indentation. The lack of lateral vents in the 25 g indentation is consistent with the surface crack geometry at this load (see Fig. 5) which shows no "radial" cracks emanating from the impression, which are the result of "penny-like" lateral cracks breaking through to the surface of the sample (Lawn and Fuller [24]).

Fig. 7 shows section micrographs of Knoop indentations made in InP at room temperature and at loads

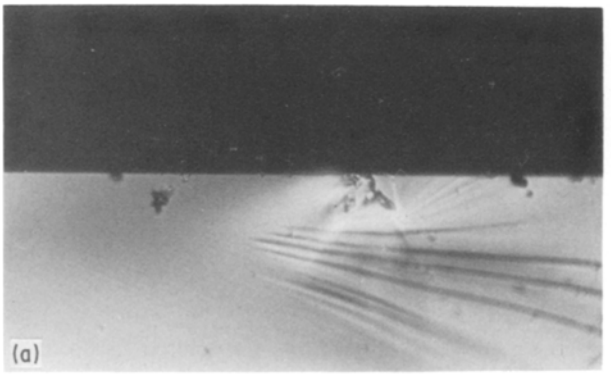

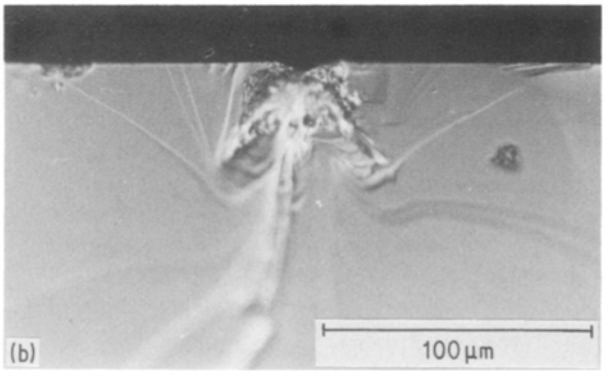

Figure 7 Cross-sectional micrographs of Knoop indentations made at room temperature in InP at loads of (a) 50 g and (b) 300 g.

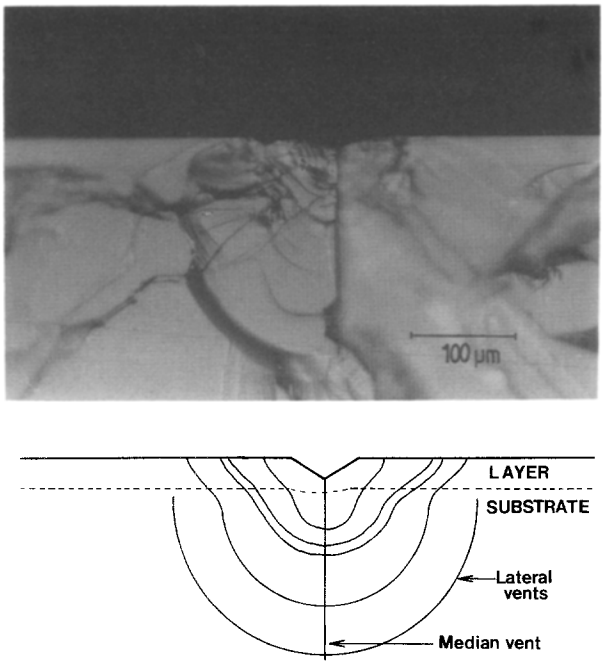

Figure 8 Cross-sectional micrograph of a 300 g load Vickers indentation made at room temperature in $In_{0.68}Ga_{0.32}As_{0.71}P_{0.29}$.

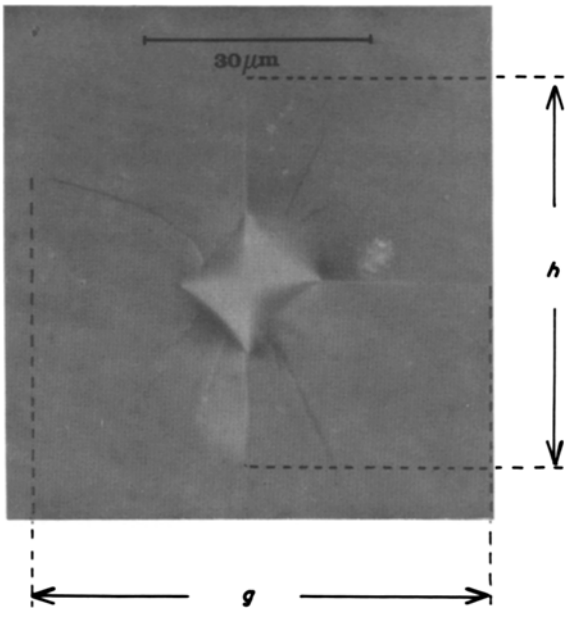

Figure 9 Typical radial fracture associated with a Vickers indentation, quantified by parameters g and h.

of 50 and 300 g. Unlike the Vickers indentations, the lateral vents appear to be the more predominant feature, at both loads although the median vent is still clearly visible.

Fig. 8 shows a section micrograph of a 300 g load Vickers indentation made at room temperature made in a 2.5 μm thick layer of $In_{0.68}Ga_{0.32}As_{0.71}P_{0.29}$ (sample Q–IGAP–6). Also shown in Fig. 8 is a clearer schematic depiction of the fracture geometry. The most important feature of the micrograph is the apparent degree of independence experienced by the sections of the lateral vents, contained within the layer material, from the remainder of the cracks confined to the bulk of the InP substrate. This independence is suggested by the clear inflexion in the "penny-like" cracks where they cross the substrate–layer interface, with the cracks in the harder (and more brittle) layer material extending further from the indentation. This suggests that measurement of the lateral vents where they intercept the surface of the layer may be used to quantify the fracture-related parameters of the layer material with minimal interference from the substrate. This "substrate-independent" fracture behaviour was also in evidence in the Knoop indentation cross-sections, and forms the premise of the quantitative fracture analysis described in Section 3.2.

3.2. Quantitative indentation fracture analysis

The aim of the quantitative indentation fracture analysis was to identify any change in fracture parameters across the $In_{1-x}Ga_xAs_yP_{1-y}$/InP system which might account for the anomalous microhardness anisotropy behaviour described in Section 1. It was decided that the measurement of the radial cracks in the surface of the sample would be the most reliable way of assessing the change in fracture characteristics: the median vent is seen to penetrate into the substrate material at low loads in even the thickest layers, and its length with therefore be largely governed by the fracture properties of InP. Measurement of the cross-sectional lateral vents is unreliable as it was established [6] that only when the cleavage of a sample was exactly along the surface radial cracks associated with the indentation were the corresponding "penny-like" cracks within the sample revealed. Finally, it was decided to concentrate on a quantitative analysis of Vickers indentation fracture, due to the increased amounts of cracking produced by this technique. The use of Vickers indentation fracture parameters to account for Knoop microhardness anisotropy data seems valid: it has already been established [6] that the $In_{1-x}Ga_xAs_yP_{1-y}$/InP system exhibits an anisotropy in Vickers hardness very similar to that in Knoop microhardness the effect merely being amplified in the latter case, and furthermore, the fracture associated with Vickers and Knoop indentation has shown similar trends. Fig. 9 shows typical radial cracks associated with a Vickers indentation together with the parameters g and h used to quantify the extent of cracking. Measurement of g and h for each indentation was achieved with the microhardness tester, using the calibrated cross-wires normally used to measure indentation dimensions. Where no cracking occurred, the values of g and h were simply the two diameters of the Vickers indentation. Indentations were made with indentor orientations of $\theta = 0°$ and 45° for each sample, with average values of $\bar{g}$ and $\bar{h}$ being derived from six separate indentations for each load, orientation and sample. The quoted cracking dimension $\bar{g}\bar{h}$ represents the average of the values of $\bar{g}$ and $\bar{h}$. The samples used had composition parameters of $y = 0.1$, $y = 0.34$, $y = 0.53$, $y = 0.7$, $y = 0.92$ and $y = 1$ (samples B–IP–1, Q–IGAP–7, Q–IGAP–8, Q–IGAP–9, Q–IGAP–6, Q–IGAP–10 and T–IGA–5, respectively). The results are summarized in Table II, all indentations having been made at room temperature with a "dwell-time" of 15 sec. Also listed in Table II for each load, indentor orientation and composition is the value of P/c (i.e. load(P)/crack dimension ($\bar{g}\bar{h}$)) in

TABLE II Radial crack length–load P/c measurements for the $In_{1-x}Ga_xAs_yP_{1-y}$/InP system

Orientation (° from ⟨1 1 0⟩)	Load (g)	Composition parameter						
		$y = 0$ (InP)	$y = 0.1$	$y = 0.34$	$y = 0.53$	$y = 0.71$	$y = 0.92$	$y = 1$ ($In_{0.53}$–$Ga_{0.47}As$)
$\theta = 0°$	25	10.65 ± 1.2	23.1 ± 1.3	23.4 ± 1.1	23.5 ± 1.1	27.1 ± 0.3	26.5 ± 1.7	23.6 ± 0.6
	50	28.6 ± 0.8	38.4 ± 1.7	39.0 ± 1.3	39.1 ± 1.2	45.1 ± 1.7	43.6 ± 1.6	41.7 ± 1.3
	100	43.1 ± 0.9	61.2 ± 2.0	63.7 ± 1.1	70.6 ± 1.9	68.6 ± 0.9	67.5 ± 3.0	66.2 ± 2.1
	200	94.0 ± 1.3	111.2 ± 1.9	110.2 ± 3.7	107.8 ± 3.1	102.7 ± 2.3	100.1 ± 3.1	99.2 ± 3.1
	300	133.0 ± 2.7	144.65 ± 2.1	147.0 ± 4.1	147.6 ± 3.0	148.0 ± 3.1	133.1 ± 2.9	133.0 ± 3.2
	500	192.4 ± 3.2	208.6 ± 3.6	207.8 ± 4.2	209.3 ± 3.2	208.3 ± 4.1	200.1 ± 5.1	194.3 ± 4.1
$\theta = 45°$	25	12.6 ± 0.9	27.4 ± 1.7	26.8 ± 0.9	24.8 ± 1.2	23.9 ± 1.2	24.7 ± 0.9	27.4 ± 0.7
	50	35.2 ± 1.6	42.5 ± 1.8	41.8 ± 1.6	41.4 ± 1.7	43.0 ± 1.7	44.1 ± 1.7	44.9 ± 1.3
	100	55.8 ± 1.2	67.3 ± 1.9	68.2 ± 1.5	70.0 ± 3.0	71.4 ± 2.1	71.0 ± 2.3	70.0 ± 1.2
	200	91.9 ± 0.8	108.55 ± 1.0	109.6 ± 2.7	113.3 ± 3.0	116.2 ± 3.0	114.2 ± 2.4	112.9 ± 3.2
	300	125.7 ± 1.7	143.3 ± 3.2	142.0 ± 2.9	139.9 ± 3.7	146.1 ± 4.1	146.0 ± 2.9	146.0 ± 3.7
	500	172.5 ± 1.8	190.1 ± 4.3	187.2 ± 4.1	186.3 ± 2.9	191.7 ± 3.9	196.4 ± 3.1	197.6 ± 4.3
P/c ($10^4 N m^{-1}$) $\theta = 0°$		2.68	2.12	2.04	1.98	1.32	1.58	1.86
P/c ($10^4 N m^{-1}$) $\theta = 45°$		1.60	1.23	1.24	1.27	1.15	1.15	1.11

*All quoted crack lengths are in μm.

units of $N m^{-1}$. The P/c values for $\theta = 45°$ indentation have been derived from the low-load region of the diagrams, as the curvature of the 45° P/c lines rules out a single unambiguous P/c value. The low load P/c values seem more appropriate because it was at these loads that the microhardness anisotropy measurements were made. These results are analysed with respect to the quantitative indentation fracture theories in Section 4.2.

4. Discussion

4.1. Quantitative indentation fracture theories

Since the establishment of the basic indentation fracture geometry for "sharp" indentors (Lawn and Swain [23]), workers have sought to quantify the extent of growth of cracks in terms of the important system variables, primarily the indentation load, P, and some characteristic crack dimension, c. It was recognized at an early stage [17] that the nucleation of cracks and their subsequent propagation were two separate phenomena requiring independent analyses. Of the two phenomena, it was crack propagation which initially attracted the most attention, and which is of interest in this work. The theories of crack nucleation are not discussed but are comprehensively reviewed by Lawn and Wilshaw [16].

Lawn and Swain [23] sought to relate P and c in terms of the mechanical constants of the material, deriving the expression

$$\frac{P}{c} = \frac{4\pi^4 \beta^2 \Gamma E}{(1 - \nu^2)(1 - 2\nu)^2 \alpha P_0} \quad (1)$$

where β is a dimensionless factor dependent on the deformation zone geometry, Γ is the fracture surface energy, E is Youngs modulus, ν is Poisson's ratio, α is the indentor geometry constant (for Vickers indentation $\alpha = 2/\pi$) and P_0 is the mean contact pressure (i.e. hardness) described by

$$P_0 = \frac{P}{\alpha \pi a^2} \quad (2)$$

where a is a measure of the zone of plastic deformation produced at the point of contact during indentation. Using typical values for these parameters for soda–lime glass, Equation 1 was seen to predict P/c characteristics which were in close agreement with experimental data. A similar expression was subsequently derived by Lawn and Wilshaw [16] which compared equally favourably with Lawn and Swains experimental data.

Lawn and Fuller [24] equated the increase in total surface energy as a crack expands to the decrease of total mechanical energy, deriving the expression

$$\frac{P^2}{c^3} = \text{const } \Gamma E \quad (3)$$

Good agreement with experimental data was observed. This equation represents the penny-like crack geometry, and a similar relation was produced by Lawn and Marshall [27]

$$\frac{P}{c^{3/2}} = \beta_0 K_c \quad (4)$$

where K_c is the fracture toughness and β_0 is a constant with an experimentally derived value of 7. Further, more complicated expressions relating and P and c have been reported (e.g. [29, 30]) but generally appear to be dependent upon prior knowledge of all the fracture-related parameters and also the appropriate choice of constants. These are not discussed here but are reviewed in [6]. Lawn and Marshall proposed the ratio H/K_c (hardness over fracture toughness) as a measure of the brittleness of a material derived by indentation. From Equations 2 and 4 this becomes

$$\frac{H}{K_c} = (\beta_0/\alpha a^{1/2})(c/a)^{3/2} \quad (5)$$

4.2. Quantitative analysis of InGaAsP fracture data

The fracture data summarized in Table II are analysed with respect to the quantitative fracture theories discussed in Section 4.1.

With the use of the appropriate values, the fracture surface energy, Γ, of InP can be derived from Equation 1, having derived P_0 from Equation 2. In Equation 2, a represents the size of the zone of plastic deformation, in this case the radius of the Vickers indentation. An extensive review of the literature produced just one value of E, for InP, reported by Wawra [31] of $E = 8.91 \times 10^{10}\,\mathrm{N\,m^{-1}}$. A value of $\nu = 0.24$ is used [32] together with values for α and β of $2/\pi$ and 2, respectively [24]. Using the $\theta = 0°$ value of P/c from Table II, a value for the fracture surface energy Γ of InP of $\Gamma = 0.0614\,\mathrm{J\,m^{-2}}$ can be calculated. Unfortunately, no independent reported value could be found in the literature with which to compare this figure. Using the low-load P/c value for $\theta = 45°$ indentation produces a value of $\Gamma = 0.04\,\mathrm{J\,m^{-2}}$ for the fracture surface energy of InP. High-load values of Γ at $\theta = 45°$ would be ambiguous due to the curvature of the $\theta = 45°$ P/c line.

Unfortunately, neither values for Γ or the Youngs modulus E could be found for the $In_{1-x}Ga_xAs_yP_{1-y}$/InP quaternary alloys and so Equation 1 cannot be used. However, it is possible to derive values for the fracture toughness, K_c, for the whole system using Lawn and Marshall's expression (Equation 4). Once again, values can be derived from the $\theta = 0°$ and 45° P/c characteristics. In the following calculations, the $\theta = 0°$ values of K_c have been calculated from the value of c at $P = 300$ g (or, more correctly, the value of c at 300 g load predicted by the line plotted through the data points; the discrepancy is quite small). However, in the case of $\theta = 45°$ indentation, the value of c at 300 g load is taken as that predicted by the low-load P/c value (see Table II) and here the discrepancy between the predicted value and the actual value is very large, because of the curvature of the $\theta = 45°$ P/c lines. It is still felt that the fracture toughness values calculated from the low-load P/c values are more realistic because they reflect the fracture behaviour in the region of loads wherein the hitherto unexplained microhardness anisotropy characteristics were measured. The variation of fracture toughness for $\theta = 0°$ and 45° Vickers indentation with composition in the $In_{1-x}Ga_xAs_yP_{1-y}$/InP system is illustrated in Fig. 10. Also shown in the diagram are the corresponding values of brittleness, determined using Lawn and Marshalls' [27] proposal that brittleness is equal to hardness divided by fracture toughness. The Vickers hardness values $\theta = 0°$ and 45° necessary to calculate the brittleness have been taken from the original report of this work [6].

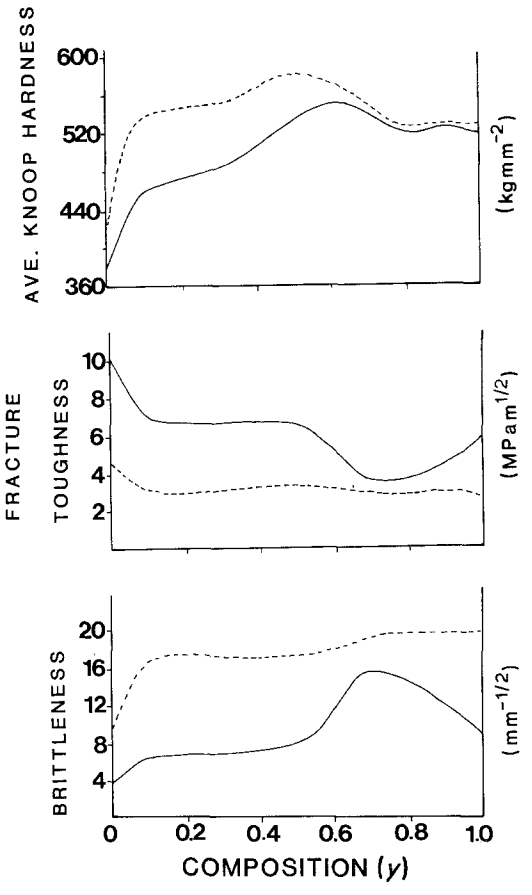

Figure 10 Variation of fracture toughness, brittleness and average Knoop hardness in the $In_{1-x}Ga_xAs_y$/InP system. (——) $\theta = 0°$, (– – –) $\theta = 45°$.

4.3. The effect of indentation fracture on hardness anisotropy

The aim of this work has been to seek an explanation for the emergence of a minimum in hardness (both Knoop and Vickers) in the $\theta = 45°$ orientation (i.e. the indentor diagonals aligned along $\langle 1\,0\,0\rangle$ directions) at high values of y in the $\{1\,0\,0\}$ oriented $In_{1-x}Ga_xAs_yP_{1-y}$/InP system. Accordingly, quantitative fracture measurements have been confined to the $\theta = 0°$ and 45° orientations.

The qualitative indentation fracture analysis revealed the emergence of what appeared to be secondary "microcleavage" cracks lying in $\langle 1\,0\,0\rangle$ directions, as the composition parameter y increased. This suggests that the $\theta = 45°$ hardness minimum might be attributable to the occurrence of this $\langle 1\,0\,0\rangle$ "cleavage" fracture, which was seen to occur as the "barrel" shape of the $\theta = 45°$ indentations gradually disappeared. The $\langle 1\,0\,0\rangle$ cleavage cracking would presumably occur at lower loads (have a lower critical stress) than the random fracture, producing the drop in hardness already seen to correspond to increased amounts of indentation fracture [33, 34]. One further point worth mentioning is that the $\theta = 45°$ Vickers indentations in $In_{0.53}Ga_{0.47}As$ (i.e. $y = 1$) produce a greater number of individual cracks at a given load than corresponding indentations in InP. For example, at 25 g load, $\theta = 45°$ Vickers indentations in $In_{0.53}Ga_{0.47}As$ produce typically 6 or 7 cracks, compared with only 2 or 3 in InP. This would further amplify any fracture-related decrease in measured hardness in the $\theta = 45°$ orientations in $In_{0.53}Ga_{0.47}As$.

The quantitative fracture analysis appears to support the above suggestion. Fig. 10 shows how the fracture toughness brittleness and average Knoop hardness in the $\theta = 0°$ and 45° orientations vary with composition in the $In_{1-x}Ga_xAs_yP_{1-y}$/InP system (calculated using the low P/c gradients). The average Knoop hardness for each orientation composition was taken from Fig. 2. The Vickers hardness in the $\theta = 0°$ and 45° orientations over the same composition range was seen to behave in a very similar manner [6] despite

the decreased reliability of the Vickers hardness measurements due to the relatively high errors at low loads. Turning to Fig. 10, it can be seen that as the hardness in both the $\theta = 0°$ and $\theta = 45°$ orientations increases sharply from $y = 0$ to $y = 0.1$, both the corresponding fracture toughness values drop. Thereafter, the more gentle rise in both hardness values corresponds to a minimal change in the fracture toughness in both orientations, although at all compositions between $y = 0$ and 1, the fracture toughness in the $\theta = 45°$ orientation is significantly less than that in the $\theta = 0°$ orientation. From $y = 0.7$ to 1.0, the fracture toughness in the $\theta = 0°$ recovers, while the value in the $\theta = 45°$ orientation continues to decrease.

The brittleness against composition diagram in Fig. 10 is perhaps more conclusive. It shows how the brittleness in the $\theta = 45°$ orientation is initially much higher than that in the $\theta = 0°$ orientation, and increases with y at a much faster rate. Furthermore, this increase is maintained to a maximum value of $y = 1$. This suggests that the size of the drop in measured hardness caused by indentation fracture will increase with increasing y continuously from $y = 0$ to $y = 1$. The $\theta = 0°$ brittleness, on the other hand, is markedly lower than that in the $\theta = 45°$ orientation at all compositions in the $In_{1-x}Ga_xAs_yP_{1-y}$/InP system, reaching a maximum at $y = 0.7$ and dropping appreciably thereafter as y increases to 1.

5. Conclusion

It is the conclusion of this work that the emergence of a minimum in both Vickers and Knoop hardness in the $\theta = 45°$ orientation (i.e. diagonals aligned along $\langle 1\,0\,0 \rangle$ directions) in $\{1\,0\,0\}$ layers of $In_{1-x}Ga_xAs_yP_{1-y}$/InP, as y increases from 0 to 1, is at least partially attributable to the marked increase in the already high brittleness in the $\theta = 45°$ orientation. This increase in brittleness is believed to give rise to both an increase in the amount of purely random indentation fracture as y increases, as well as the emergence of what appears to be a secondary microcleavage direction along $\langle 1\,0\,0 \rangle$. It is the large increase in the amount of fracture in the $\theta = 45°$ orientation as y increases (and at angles approaching $\theta = 45°$) which is believed to produce the low hardness values which are seen as a minimum in the Knoop hardness anisotropy curves of high-y $In_{1-x}Ga_xAs_yP_{1-y}$/InP. Of course, the general effect of the composition on hardness is related to the effects of many phenomena, particularly solid solution hardening, but this work establishes that, even at very low indentation loads, indentation fracture may have a profound effect upon the hardness characteristics of brittle crystalline materials.

Acknowledgements

The work in this paper was supported by the SERC, and the authors would like to acknowledge the valuable assistance of Mr A.C. Riddell and the Engineering Materials workshop. The InGaAsP samples were kindly supplied by Dr P. D. Greene (STL, Harlow).

References

1. D. Y. WATTS and A. F. W. WILLOUGHBY, *J. Appl. Phys.* **56** (1984) 1869.
2. *Idem, Mater. Lett.* **2** (1984) 355.
3. *Idem,* Proceedings 13th International Conference on Defects in Semiconductors, Coronado, California, edited by L. C. Kimmerling and J. M. Parsey, The Metallurgical Society of AIME, 12–17 August, 1984, pp. 1187–94.
4. D. BRASEN, *J. Mater. Sci.* **11** (1976) 791.
5. *Idem, ibid.* **13** (1978) 1776.
6. D. Y. WATTS, PhD thesis (1986).
7. F. W. DANIELS and C. G. DUNN, *Trans. Amer. Soc. Met.* **41** (1949) 419.
8. C. FENG and C. ELBAUM, *Trans. Met. Soc. AIME* **212** (1958) 47.
9. C. A. BROOKES, J. B. O'NEILL and B. A. W. REDFERN, *Proc. Roy. Soc. A* **322** (1971) 73.
10. M. GARFINKLE and R. G. GARLICK, *Trans. Met. Soc. AIME* **242** (1968) 809.
11. G. Y. CHIN and W. A. HARGREAVES, in "The Science of Hardness testing and its research applications", edited by J. H. Westbrook and H. Conrad, Symposium Proceedings (American Society of Metals, Detroit, 1971) ch. 12.
12. S. KOMIYA and K. NAKAJIMA, *J. Crystal Growth* **48** (1980) 403.
13. O. UEDA, S. KOMIYA, S. YAMAZAKI, Y. KISHI, I. UMEBO and T. KOTANI, *Jpn J. Appl. Phys.* **23** (1984) 836.
14. J. A. LOURENCO, *J. Electrochem. Soc.* **131** (1984) 1914.
15. D. TABOR, *Rev. Phys. Technol.* **1** (1970) 145.
16. B. R. LAWN and T. R. WILSHAW, *J. Mater. Sci.* **10** (1975) 1049.
17. C. A. BROOKES, *Nature London* **228** (1970) 660.
18. H. HERTZ, *J. Reine Angew Matt.* **92** (1881) 156.
19. J. BOUSSINESQ, "Application des Potentials a l'Etude d'equilibre et du mouvement des solides elastiques" (Gauthier-Villars, Paris, 1885).
20. S. PALMQVIST, *Arch. Eisenhuttenw.* **33** (1962) 629.
21. M. T. HUBER, *Ann. Physik* **14** (1904) 153.
22. H. E. EXNER, *Trans. Met. Soc. AIME* **245** (1969) 677.
23. B. R. LAWN and M. V. SWAIN, *J. Mater. Sci.* **10** (1975) 113.
24. B. R. LAWN and E. R. FULLER, *ibid.* **10** (1975) 2016.
25. B. J. HOCKEY and B. R. LAWN, *ibid.* **10** (1975) 1275.
26. D. B. MARSHALL and B. R. LAWN, *ibid.* **14** (1979) 2001.
27. B. R. LAWN and D. B. MARSHALL, *J. Amer. Ceram. Soc.* **62** (1978) 347.
28. S. G. ROBERTS, P. PIROUZ and P. B. HIRSCH, *J. Mater. Sci.* **20** (1985) 1739.
29. B. R. LAWN and A. G. EVANS, *ibid.* **12** (1977) 2195.
30. A. G. EVANS and E. A. CHARLES, *J. Amer. Ceram. Soc.* **59** (1976) 371.
31. I. H. WAWRA, *Blech Rohre* **8** (1975) 333.
32. M. BEUBERGER, (ed.) "Handbook of Electronic Materials", Vol. 2 (IFI/Plenum, New York, 1971).

Received 19 March
and accepted 15 March 1987